



Development of self-tuned diamond milling system for fabricating infrared micro-optics arrays with enhanced surface uniformity and machining efficiency

ZHANWEN SUN,¹ SUET TO,² SUJUAN WANG,^{1,*} AND JIANJUN DU³

¹State Key Laboratory of Precision Electronic Manufacturing Technology and Equipment, Guangdong University of Technology, Guangzhou, China

²State Key Laboratory in Ultra-precision Machining Technology, Department of Industrial and Systems Engineering, The Hong Kong Polytechnic University, Kowloon, Hong Kong

³School of Mechanical Engineering and Automation, Harbin Institute of Technology Shenzhen, Shenzhen, 518055, China

*grace.wangsj@gdut.edu.cn

Abstract: Infrared micro-optics arrays (MOAs) featuring large numbers of micro-freeform lenslet are required increasingly in advanced infrared optical systems. Ultra-precision diamond cutting technologies have been widely used to fabricate MOAs with high form accuracy. However, the existing technologies can easily cause the non-uniformly fractured surface of infrared MOAs, due to the inherent low fracture toughness and high anisotropy of infrared materials as well as the time-varying chip thickness induced by ever-changing height and slope of the desired MOAs. In this study, a novel self-tuned diamond milling (STDM) system is proposed to achieve the ductile cutting of infrared MOAs with enhanced the surface uniformity and machining efficiency, and the corresponding toolpath planning algorithm is developed. In STDM system, a dual-axial fast servo motion platform is integrated into a raster milling system to self-adaptively match the maximum chip thickness for each tool rotational cycle with the critical depth of cut of the infrared material according to the local surface topography, thereby obtaining crack-free lenslet with high surface uniformity. Practically, micro-aspheric MOAs free from fractures are successfully machined on single-crystal silicon, a typical infrared material, to validate the proposed cutting concept. Compared with the conventional diamond milling, the proposed STDM is demonstrated to be able to avoid the non-uniform fractures without needing to reduce feed rate, and a smaller surface roughness of 4 nm and nearly double machining efficiency are achieved.

© 2020 Optical Society of America under the terms of the [OSA Open Access Publishing Agreement](#)

1. Introduction

Infrared micro-optics arrays (MOA) has found widespread applications in infrared optical systems, photonic devices and sensors, attributing to its superiorities in high sensitivity, minimization and side field of view [1,2]. These infrared MOAs are generally characterized as discontinuous micro-structured surfaces consisting of periodically arranged lenslet cells. Currently, the shape of the lenslet has developed from simple spherical surfaces to aspherical or even micro-freeform surfaces, to realize the specific functions of various applications [3,4]. However, most infrared optical materials, such as germanium and silicon, are characterized as very low fracture toughness and high anisotropy. The increasing complexity of the micro-structured lenlet together with the hard-and-brittle properties of infrared materials impose new challenges for the existing machining techniques to realize the flexible generation of infrared MOAs with smooth and uniform surface quality as well as with enhanced machining efficiency. It is known that the infrared optical components should not only have smooth surface quality with high form accuracy, but also have high surface uniformity to avoid imaging distortion and undesired scattering effect [5,6].

Currently, both non-mechanical and mechanical techniques have been employed for the manufacturing of MOAs on infrared materials. For the non-mechanical methods, mainly including lithographic technologies and chemical etching, their common advantage is the capability of manufacturing large quantities of lenslet cells [7,8]. Nevertheless, most of these methods are restricted to generating the lenslet with entrenched feature sizes and limited geometries on specified materials, and complex operations are normally required to obtain satisfactory surface quality. Thus, the lack flexibility and the uncontrollable factors of the non-mechanical methods set up a barrier to fulfil the increasing requirement of infrared MOAs.

Compared with the non-mechanical methods, mechanical machining technologies, dominated by fast and slow tool servo (FTS/STS) diamond turning and multi-axis diamond milling, provide a more flexible and deterministic way to fabricate infrared MOAs featuring complicated micro-freeform surfaces with high form accuracy. Developed from diamond turning, FTS/STS diamond cutting employs translational servo motions along z -axis to generate aspheric and micro-freeform lenslet cells with sub-micro form accuracy and nano-metric surface roughness [9,10]. Although FTS/STS has been demonstrated to be an outperforming technique, it is still challenging for the fabrication of infrared MOAs with crack-free and uniform surface quality, attributing to some inherent defects of FTS/STS. Specifically, as FTS/STS is operated in Cylindrical coordinate system, its cutting directions constantly changes relative to the crystal orientations of single-crystal infrared materials, which is prone to form radial-spoke marks and inhomogeneous cracks on infrared lenslet, accordingly damaging the optical performance [11,12]. Additionally, the inevitable tool vibrations induced by the discontinuous toolpath adopted in FTS/STS turning of MOAs can significantly deteriorate the surface roughness by printing tool marks on the finished lenslet surfaces [13]. Especially, with increasing complexity and the aspect ratio of the lenslet, the tool vibrations can be more severe. On the other hand, the ever-changing cutting velocity, cutting forces and the azimuth sampling conflicts induced by the time-varying radial distance of the cutting point in FTS/STS can result in the high sensitivity of the finished surface quality to the position of the lenslet on the MOAs [14,15]. To enhance the surface uniformity and to avoid fractures on the finished surfaces, extremely small feed rate needs to be deliberately selected for FTS/STS to suppress tool vibration and to guarantee ductile removal of infrared materials, resulting in the low machining efficiency.

Multi-axis diamond milling can be divided into two main types according to the installing method of the diamond tool, namely ball end milling and raster milling [16–18]. In ball end milling, three translational sides drives the rotational ball milling tool to generate lenslet cells one by one, accordingly forming the whole MOAs. Even though ball end milling can provide the consistent cutting process from the view of the whole MOAs, this method is difficult to guarantee the surface uniformity and smoothness within one lenslet cell, due to the easy occurrence of brittle fractures at the bottom surface of each lenslet where the instantaneous cutting depth is larger than a critical value. Besides, the relatively large gyration radius of ball milling tool highly limits the geometric complexity and the density of lenslet cells. By contrast, in raster milling, also named as fly cutting, a diamond turning tool or an insert diamond tool is adopted instead of a ball milling tool, and its rational axis is parallel to the workpiece surface. Compared with F/STS and ball end milling, raster milling has a totally different ductile machining model [19] and has been demonstrated to be more beneficial to the ductile machining of infrared materials for micro-structured surfaces, attributing to its two main advantages: (i) the intermittent cutting process can efficiently suppress the cracks of infrared material by generating very small chip thickness [20]; (ii) the unchanged cutting direction reduce the undesired radial-spoke marks generated in FTS/STS of single-crystal infrared materials [16]; (iii) the multi-axes cutting nature of milling effectively avoid the tool vibrations even when machining MLAs with complicated geometries. Attributing to the abovementioned advantages together with its high flexibility and

high form accuracy, multi-axis raster milling has attracted ever-increasing attentions to fabricate infrared optics featuring micro-structured or even micro-freeform surfaces.

In raster milling of MOAs, the maximum chip thickness for each tool rotational cycle jointly depends not only on the factors for cutting planer surfaces, such as feed rate, cutting depth and tool geometries, but also on the local slope of the desired MOAs. To obtain smooth surfaces, two essential conditions should be fulfilled: (i) the infrared materials are removed in completely ductile mode, which can be realized through strictly restricting the chip thickness to be less than the critical depth of cut (DoC) that is defined as the cutting depth at which the ductile-to-brittle transition originate; or (ii) the cracks generated at slightly larger feed rates is totally removed by the subsequent tool passes without propagating into the finished surfaces. Even though the critical DoC of infrared materials is influenced by the tool rake angle and cutting directions, the value is normally in the range of sub-micrometers [21]. Accordingly, extremely small feed rate is generally required to guarantee the overall smoothness of the infrared lenslet, which is applicable to the lenslet with simple shapes and gentle slope variation. Nevertheless, the increasing complexity of the micro-structured and micro-freeform surfaces inevitably leads to the inconsistent cutting process featuring ever-changing chip thickness from position to position, thereby easily inducing the non-uniform surface quality featuring local fractures of the machined surfaces. Besides, the ever-changing height and local slope of a micro-freeform surface results in the difficulty to accurately estimate the fractured positions and to select appropriate machining parameters. The currently adopted strategy using a sufficiently small feed rate to avoid fractures at the largest DoCs of a micro-freeform surface is over inefficient for the areas with smaller DoCs, thereby significantly reducing the machining efficiency. A similar bottleneck also happens in FTS/STS and ball milling of infrared MOAs.

As the critical DoC is an important factor related to the surface uniformity and machining efficiency, a variety of methods have been proposed to increase the critical DoC of infrared materials, such as vibration-assisted cutting [22], laser-assisted cutting [23] and ion implantation modification [24]. With the assistance of the extra energy, vibration-assisted and laser-assisted cutting have been demonstrated to be effective to improve the machinability of infrared materials by enhancing its plastic deformation, thereby suppressing brittle fractures even under slightly higher cutting depths. It is also reported that ion implantation modification is beneficial to increase the critical DoC of infrared materials through modifying a thin layer of the workpiece surface. Although the integration of these methods into the ultra-precision diamond cutting technologies can effectively enhance surface quality and machining efficiency for the generation of infrared MOAs, the inherent process inconsistency of the existing technologies is still not improved as these methods ignore the geometric features of the micro-freeform lenslet and cannot self-adaptively tune the chip thickness according to the local surface topography of the micro-freeform surface.

Facing the above dilemmas, the development of new machining systems with self-tuned nature is needed to guarantee the cutting consistency and smoothness of the whole infrared MOAs, thereby enhancing the surface uniformity and machining efficiency. In this study, a novel self-tuned diamond milling (STDm) system is proposed by integrating a dual-axial fast servo motion platform into a raster milling system, to achieve the flexible generation of infrared MOAs with high surface uniformity and enhanced machining efficiency. Unlike the existing diamond cutting technologies that only consider the form accuracy of the desired micro-freeform surfaces, the STDm employs the dual-axial fast servo motion to self-adaptively and flexibly adjust the chip thickness according to the local surface topography, accordingly guaranteeing process consistency. The corresponding toolpath planning algorithm is also proposed with the full consideration of the unique kinematics of the STDm system, the infrared material property and the tool geometry. In practical, micro-aspheric MOAs are machined on single-crystal silicon, and the experimental

results were compared with that obtained by conventional raster milling to validate the proposed STDM.

2. Machining principle for self-tuned diamond milling

To avoid brittle fractures of infrared MOAs in diamond milling, the most reliable way is to remove the infrared material in ductile mode. This is able to be realized through restricting the maximum chip thickness for each tool rotational cycle to be no larger than the critical DoC of the infrared material. In diamond milling of MOAs featuring complicated micro-freeform surfaces, the maximum chip thickness for each tool rotational cycle depends not only on the machining parameters for cutting planer surfaces, such as feed rate and DoC, but also on the local slope of the desired MOAs. Thus, the geometric complexity of the micro-freeform surfaces inevitably leads to the ever-changing chip thickness with cutting positions, thereby resulting in the easy formation of brittle fractures and the difficulties to select appropriate machining parameters in conventional milling. The current solution using an extremely small feed rates will highly reduce the machining efficiency. To overcome this bottleneck, a self-tuned diamond milling (STDM) system is proposed through integrating a dual-axial fast servo motion platform into a raster milling system.

Figure 1(a) schematically illustrates the hardware configuration of the STDM system. A diamond tool is installed on a tool holder then fixed on the aerostatic bearing spindle, whereas the workpiece is attached on the end-effector of a three degree-of-freedom (DoF) fast servo motion platform and then fixed on the y -axis slide. The three-DoF motion platform constructed by three sets of decoupled compliant mechanisms can generate fast servo motions along x -, y - and z -axis, but only the servo motions along feed (x -axis) and DoC (z -axis) directions are used in the proposed STDM system. The schematic of the cutting motions is illustrated in Fig. 1(b). During machining, the spindle rotates and feeds along x -axis with a constant moving speed, and the diamond tool intermittently cuts into and out of the workpiece to remove the material. With the assistance of the three-DoF motion platform, the workpiece follows the fast servo motions along z -axis, just like fast FTS, to generate the desired micro-structured surfaces. Simultaneously, an extra fast servo motion is also imposed on the workpiece along feed (x -axis) direction to strictly match the maximum chip thickness with the critical DoC according to the local surface topography, thereby obtaining crack-free micro-freeform surfaces with high uniformity as well as improving machining efficiency. Through repeating this cutting operation along the y -axis with a step movement, just like raster milling, the whole workpiece can be covered, and desired

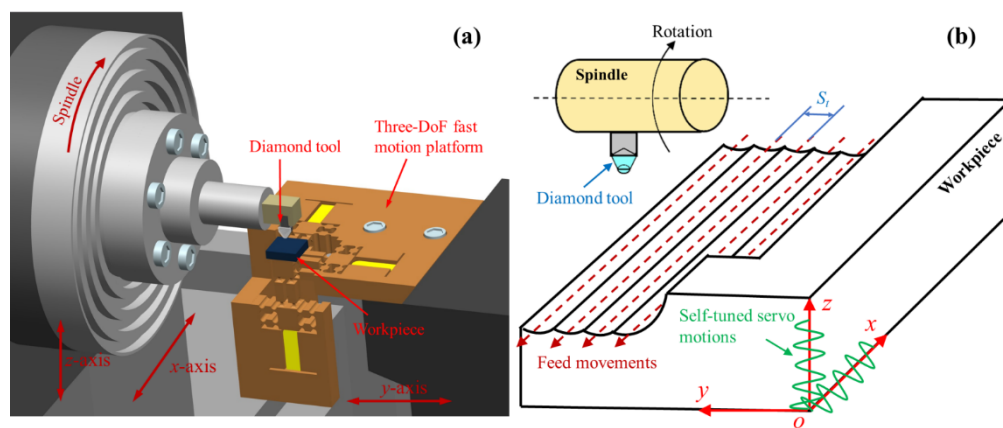


Fig. 1. Schematic of (a) hardware configuration and (b) cutting mechanism of STDM.

MOAs can be obtained. The whole lens array is generated by a few raster cutting cycles on a plane surface, as illustrated in Fig. 1(b), instead of cutting each lenslet cell one by one.

Apart from the common advantages of diamond milling technique in manufacturing of MOAs, such as high flexibility and constant cutting speed, the unique machining principle of STDM system also provides the following advantages:

- (i) Avoidance of the local fractures in manufacturing of infrared MOAs with complicated micro-freeform surfaces. In STDM system, through deliberately controlling the extra servo motion along x -axis, the instantaneous feed rate is able to be adjusted in real time according to the local shape feature of the desired micro-freeform surfaces, in which way the maximum chip thickness for each tool rotational cycle is constant without being influenced by the ever-changing DoCs and local slope of the lenslet, as the illustrated in Figs. 2(a) and 2(b). Through actively setting the maximum chip thickness to be a value no larger than the critical DoC, brittle fractures can be efficiently avoided throughout the whole MOAs. In contrast, the feed rate for conventional milling is non-adjustable and unchanged during cutting process, so the maximum chip thickness changes from position to position, as illustrated in Figs. 2(b) and 2(c), which is the main reason resulting in the non-uniformly distributed brittle fractures of infrared MOAs;

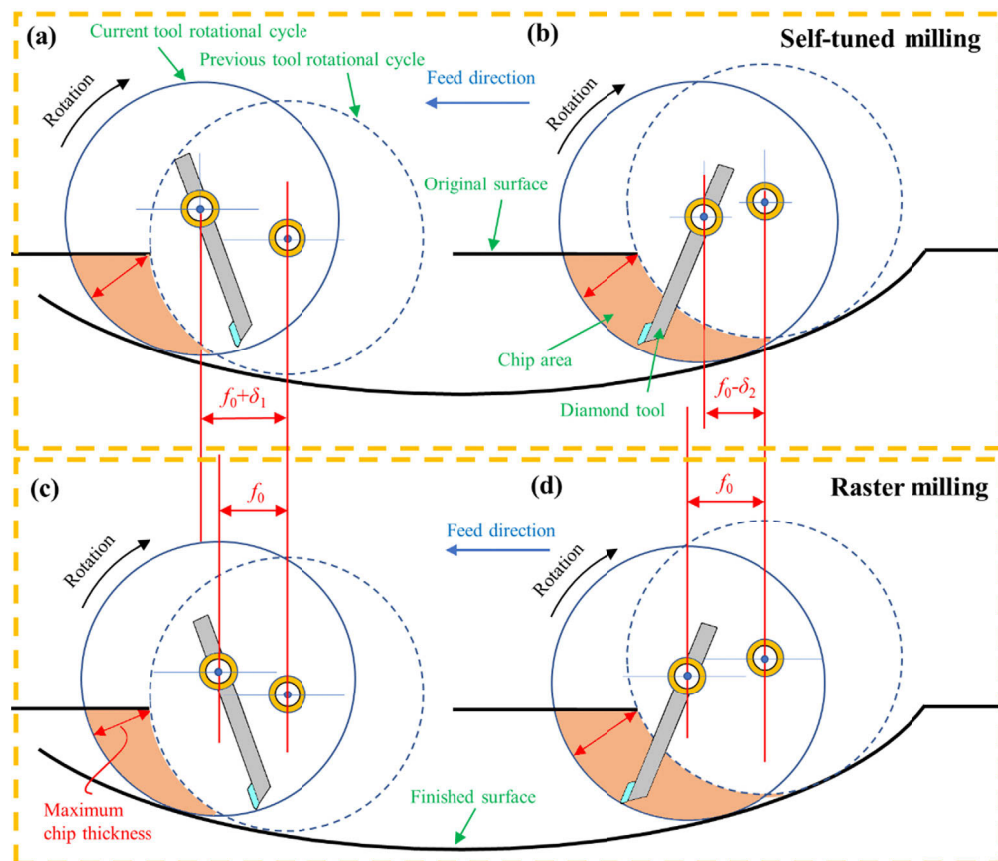


Fig. 2. Schematic of the chip formation under (a) and (b) STDM and (c) and (d) conventional raster milling.

- (ii) Improvement of the machining efficiency. The currently adopted strategy using small feed rates to guarantee the ductile material removal at the largest DoC of a micro-freeform surface extremely limits the machining efficiency for conventional diamond milling. In comparison, the self-tuned adjustment of the chip thickness for STDM allows a much higher average feed rate while avoids fractures, thereby improving the machining efficiency.

3. Toolpath determination for STDM

3.1. Toolpath planning algorithm

Different from conventional diamond milling that only includes three-axis servo motions, the proposed STDM employs an extra fast servo motion along x -axis to actively tune the maximum chip thickness according to the local surface topography, so a more complicated toolpath planning algorithm is required for STDM. According to the machining principle of STDM, the toolpath planning algorithm is developed through numerically determining a group of the swing center points (SCPs) of the spindle under the constraints of both the form accuracy of the desired micro-freeform surface and the accordance between the maximum chip thickness and critical DoC. Then, according to the determined coordinates of SCPs, the servo motions of the fast motion platform along the x - and z -axis are accordingly determined.

In STDM, the rotating spindle alternatively moves along feed (x -axis) and raster (y -axis) directions in STDM to finally generate the desired micro-freeform surfaces. Assuming the original surface of infrared material is planar, a coordinate system $o-xyz$ is built on the workpiece with the x - and y -axis pointing to the feed and raster directions, as shown in Fig. 1(b). By means of the equal interval based discretization, the workpiece is evenly divided into N pieces along raster direction, so the projected toolpath in $o-xy$ plane is a group of straight lines that are parallel distributed along raster direction with a fixed interval of S_r , as shown in Fig. 1(b). Accordingly, the y coordinate of the i -th SCP located in the j -th feed motion cycle can be denoted in the workpiece coordinate system as:

$$y_{i,j}^{(w)} = j \cdot S_r \quad (1)$$

In STDM, the chips are intermittently formed by two neighboring tool rotational cycles along feed direction, as illustrated in Fig. 3(a). Unlike milling planar surface, the maximum chip thickness for the milling of micro-freeform surfaces is determined not only by the machining parameters, but also by the local slope of the desired surface as well as the position of the SCP in the previous tool rotational cycle, namely the position of $P_{i-1,j}$ in Fig. 3(a). As the 3D schematic

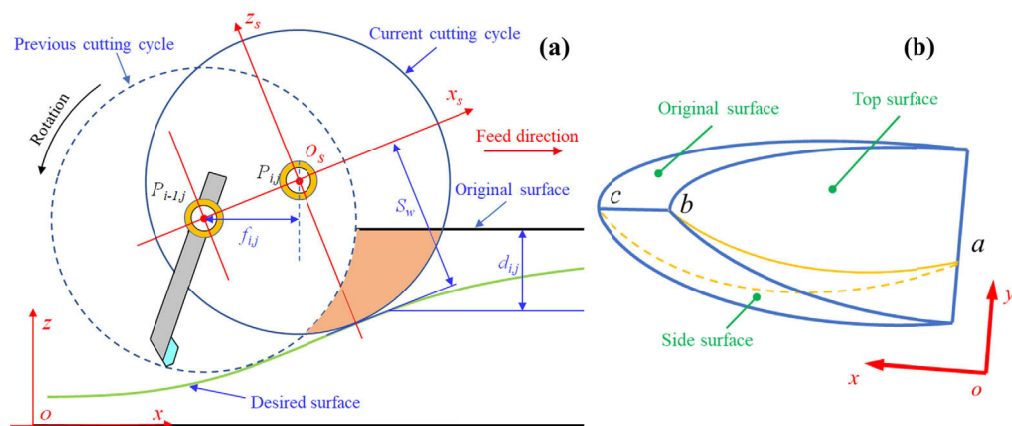


Fig. 3. Schematic of (a) STDM viewed from y -axis and (b) 3D morphology of the chip.

morphology of the chip formed by STDM shown in Fig. 3(b), each piece of chip is enveloped by four surfaces, namely the original, top, bottom and side surfaces. It is learned that the chip thickness changes from zero at the tool-workpiece contacting point a to the maximum value at point b , and then back to zero again at point c . Thus, the maximum chip thickness is able to be determined by directly calculating the distance between point c and the intersection point between the bottom surface of the chip and the straight line connecting the points c and $P_{i,j}$.

Another coordinate system $o_s-x_s y_s z_s$ is built on the swing center of spindle with its x_s -axis parallel to the desired surface, as shown in Fig. 3(a). As the interval between to neighboring cutting cycle is very small, so the slope change can be neglected, and as the cutting duration for each tool rotation is very short in STDM, the spindle is assumed to have no movement during chip formation to simple the calculation. According to the geometrical relation, the coordinate $(x_b^{(s)}, y_b^{(s)}, z_b^{(s)})$ of the point b in the spindle coordinate system can be obtained by solving the following equations as:

$$\begin{cases} x_b^{(s)} = \sqrt{(\sqrt{R_t^2 - (y_b^{(s)})^2} + S_w - R_t)^2 - (z_b^{(s)})^2} - f_{i,j} \\ y_b^{(s)} = \frac{z_b^{(s)} \cos \theta_{i,j} - d_{i,j} + S_w \cdot \cos \theta_{i,j}}{\sin \theta_{i,j}} \\ z_b^{(s)} = R_t - S_w + S_t \sin \varphi_{i,j} - \sqrt{R_t^2 - (y_b^{(s)} - S_t \cos \varphi_{i,j})^2} \end{cases} \quad (2)$$

where R_t is the tool nose radius, S_w is the tool swing radius and $d_{i,j}$ is the instantaneous cutting depth. $\theta_{i,j}$ and $\varphi_{i,j}$ are the inclination angle of the desired surface along the x_s - and y_s -axis, respectively, which are expressed as:

$$\begin{cases} \theta_{i,j} = \arctan\left(\frac{z_{i,j}^{(w)} - z_{i-1,j}^{(w)}}{f_{i,j}}\right) \\ \varphi_{i,j} = \arctan\left(\frac{z_{i,j}^{(w)} - z_{i,j-1}^{(w)}}{S_t}\right) \end{cases} \quad (3)$$

The expression of the straight line connecting the points c and $P_{i,j}$ is given as:

$$\frac{x}{x_b^{(s)}} = \frac{y}{y_b^{(s)}} = \frac{z}{z_b^{(s)}} \quad (4)$$

The coordinate of the intersection point $(x_i^{(s)}, y_i^{(s)}, z_i^{(s)})$ between the bottom surface of the chip and the straight line can be determined by Eqs. (2) and (3) as:

$$\begin{cases} x_i^{(s)} = x_b^{(s)} \cdot k \\ y_i^{(s)} = y_b^{(s)} \cdot k \\ z_i^{(s)} = z_b^{(s)} \cdot k \end{cases}, k = \frac{(S_w - R_t) \sqrt{(x_b^{(s)})^2 + (y_b^{(s)})^2} + \sqrt{R_t^2 (x_b^{(s)} + z_b^{(s)})^2 + (y_b^{(s)})^2 S_w (S_w - 2R_t)}}{(x_b^{(s)})^2 + (y_b^{(s)})^2 + (z_b^{(s)})^2} \quad (5)$$

Based on Eqs. (2) and (5), the maximum chip thickness h_{\max} for the i -th SCP located in the j -th feed motion cycle is denoted as:

$$h_{\max} = \sqrt{(x_b^{(s)} - x_i^{(s)})^2 + (y_b^{(s)} - y_i^{(s)})^2 + (z_b^{(s)} - z_i^{(s)})^2} \quad (6)$$

It is known that the critical DoC is the threshold value that differentiate the ductile and brittle material removal. Thus, through replacing maximum chip thickness h_{\max} by the critical DoC of the infrared material in Eq. (6), the overall smoothness of the generated MOAs without brittle fractures can be well guaranteed while maximumly improving the machining efficiency.

From Eqs. (2)–(6), it is known that the position of $P_{i,j}$ is iteratively determined by the points of $P_{i-1,j}$ and $P_{i,j-1}$, and there are two unknown variables, namely $f_{i,j}$ and $z_{i,j}$ in these equations. To determine namely $f_{i,j}$ and $z_{i,j}$, another equation that describing the tangency between the surface formed by the tool rotation at $P_{i,j}$ and the desired micro-freeform surface is required to be established. Through evenly dividing the tool rotational trajectory into $2N_s$ pieces and tool edge into $2N_t$ pieces, the surface formed by the tool rotation at $P_{i,j}$ can be denoted as:

$$z_{m,n}^{(s)} = \sqrt{\left(R_t \sqrt{1 - \left(\frac{n}{N_t}\right)^2} + S_w - R_t\right)^2 - \left(\frac{mS_w}{N_s}\right)^2}, m \in [-N_s, N_s], n \in [-N_t, N_t] \quad (7)$$

The tangency condition can be simplified by calculating the minimum distance between the surface described by Eq. (7) and the desired surface, so the other mathematical relation between the two unknown variables, namely $f_{i,j}$ and $z_{i,j}$, can be expressed as:

$$z_{i,j} = \min \left| z_{m,n}^{(s)} - F\left(f_{i,j} + x_{i-1,j} + \frac{m}{N_s} S_w, y_{i,j}^{(w)} + \frac{n}{N_t} R_t\right) \right| + z_0, \forall m \in [-N_s, N_s], \forall n \in [-N_t, N_t] \quad (8)$$

where z_0 is the virtual distance and $F(\cdot)$ denotes the function of the desired lenslet surface. By solving Eqs. (6) and (8), the positions of all SCPs are able to be iteratively determined considering of the material property, unique kinematics, form accuracy of the desired surface and tool geometry. The first SCP is located at the top and right corner of the workpiece, and a constant feed rate is used to determine the SCPs at the first feed cutting cycle, and these SCPs are employed as the basic data for the following iterative calculation. It is worth to note that even though the transition area between lenslet and plane surface is not continuous, the tangency condition described in Eq. (8) can well guarantee the smooth transition without overcut.

3.2. Characteristics of the toolpath

To characterize the machining process of STDm, the toolpath of typical micro-aspheric MOAs is determined by the above-mentioned toolpath planning algorithm, as shown in Fig. 4(a). Figure 4(b) shows the shape feature of the MOAs. The aperture and height of each lenslet cell are 500 μm and 4 μm , respectively. In order to have a clearer view, the projected view of the toolpath on x - y plane is shown in Fig. 4(c). It is observed that a much denser SCPs are distributed at the areas corresponding to lenslet cell in comparison with the planar surface. The time interval between two neighboring points is fixed in the figures, which indicates smaller feed rates during machining lenslet cells. To better characterizing the toolpath for STDm, a comparison of the distribution of SCPs for the central line of an arbitrary lenslet along feed direction between the self-tuned and conventional raster milling is illustrated in Fig. 4(d). It is obvious that the density of SCPs for STDm changes with respect to the instantaneous cutting depth and local slope of the lenslet, and the density of the SCPs at downward slope is obviously higher than that at upward slope even under the same cutting depth. This validates the effectiveness of the proposed toolpath planning algorithm in terms of the adaptive adjustment of the feed rate to match the maximum chip thickness with the critical DoC. In comparison, the spacing distance between two neighboring SCPs for conventional raster milling is unchanged throughout the machining process, which is accordingly prone to inducing the brittle fractures of lenslet at the downward and deep areas.

In order to explain the motion characteristics of STDm, the relative motion between the SCP and the workpiece along feed direction for a raster cutting cycle is depicted in Fig. 5(a). It features a linearly increasing tendency with the imposition of periodic fluctuations. As learned from the machining principle of STDm, this is due to the reason that the motion of SCP relative to the workpiece is the resultant motion of both the uniform motion of the spindle and the self-tuned

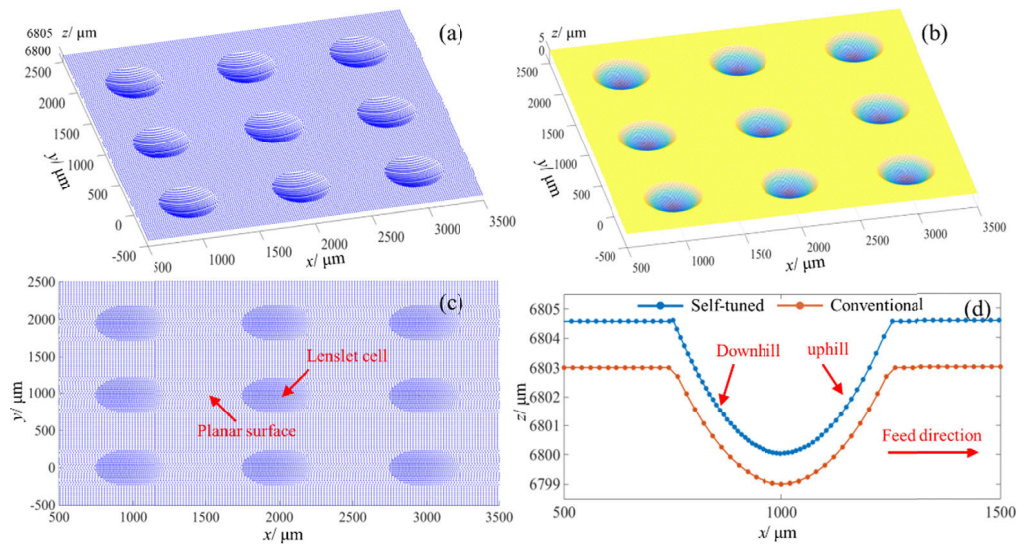


Fig. 4. Schematic of (a) toolpath and (b) shape of micro-aspheric arrays, (c) toolpath in x - y plane and (d) distribution of SCPs for the central line of one lenslet.

servo motion of the fast motion platform, which are depicted in Figs. 5(b) and 5(c), respectively. Due to the self-tuned motion, the instantaneous feed rate for STDM also periodically fluctuates at different positions along x -axis, as the blue line shown in Fig. 5(d). The feed rate is calculated though dividing the distance between two neighboring SCPs by the fixed time interval. Assuming the spindle speed is 6000 rpm and the critical DoC is 100 nm, the calculated average feed rate for STDM is 22.4 mm/min, while the minimum feed rate is 11.3 mm/min. Under the same cutting conditions, the maximum feed rate allowed in conventional raster milling need to be less than 11.3 mm/min to avoid the brittle fractures at the largest DoC region. Therefore, the machining efficiency of STDM is nearly twice as much as that of conventional milling.

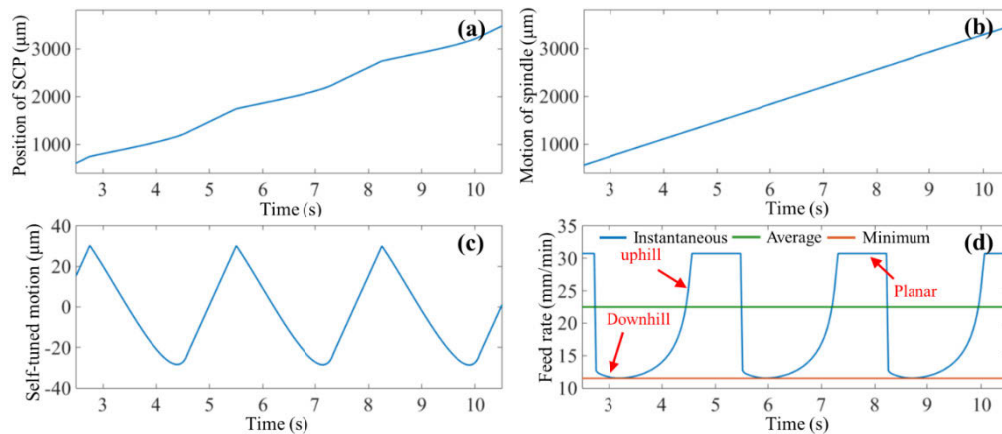


Fig. 5. (a) Position of the SCPs along feed direction, motions of the (b) spindle and (c) self-tuned platform in x -axis and (d) feed rate.

4. Development of STDM system and experimental setup

With reference to Fig. 1(a), the STDM system is developed through assembling a three-DoF piezo-actuated motion platform on a CNC ultra-precision lathe (Moore nanotech 350FG) with three translational motion slides and a rotational spindle, as shown in Fig. 6(a). As shown in Fig. 6(b), the three-DoF motion platform is actuated by three piezo-actuators, and three unidirectional compliant mechanisms configured in an orthogonal way is used to accurately guide the motions in each direction. The machining principle of STDM is detailed in Section 2. In the machining process, the CNC lathe is controlled like raster milling a planar surface, and the positions of x - and y -slides are constantly monitored and transmitted to a multi-axis motion control card (Power PMAC) to guarantee the synchronous motions between the CNC lathe and the piezo-actuated motion platform. Subsequently, based on the gathered positions and the planned toolpath, control signals are generated by PMAC control card, and input into the piezo-actuators after being amplified by the power amplifiers. The displacement of the end-effector along feed and DoC directions are gathered by PMAC using a capacitive position sensor for feedback control. Consequently, the STDM of infrared MOAs can be achieved by the synchronous control of both the multi-axis CNC lathe and the piezo-actuated motion platform.

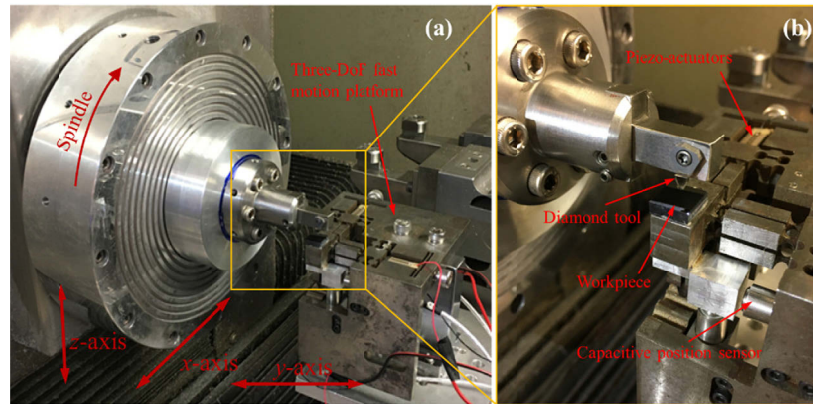


Fig. 6. (a) Hardware configuration of the STDM system and (b) an enlarged view of the three-DoF fast motion platform.

To validate the proposed STDM, micro-aspheric MOAs were fabricated on single-crystal silicon. Silicon is the infrared material that is widely used on advanced infrared optical systems. Based on the taper cutting experiment, the critical DoC of single-crystal silicon along $\langle 110 \rangle$ crystal direction is determined at ~ 120 nm [25], so the critical DoC adopted in toolpath planning is 100 nm in this study to guarantee the ductile material removal mode. A round-edged diamond tool with a nose radius of 0.5 mm is adopted in experiments. The rake angle and clearance angle of the tool are -25° and 7° , respectively. The micro-scope images of the machined MOAs were also captured by the optical micro-scope system (Olympus BX60). The non-contact optical surface profiler (Nexview, Zygo) is adopted to capture the topographies and the form accuracy of the generated MOAs. The mathematical description of the micro-aspheric lenslet cell is [26]:

$$z(x, y) = \frac{sCR_0^2}{4 + 4\sqrt{1 - (1+k)C^2R_0^2}} - \frac{sC\rho^2(x, y)}{4 + 4\sqrt{1 - (1+k)C^2\rho^2(x, y)}} \quad (9)$$

where C is the constant controlling the curvature, R_0 is the radius of each lenslet, k defines the conic surface where $-1 < k < 0$ for aspheric surfaces, s controls the convex or concave surface and ρ denotes the radial distance in local coordinate system. The coefficients defining the shape of

the machined micro-aspheric lenslet cell in this study is listed in Table 1. For comparison, both STDM and conventional diamond milling were used to fabricate the micro-aspheric MOA, and the machining parameters as listed in Table 2.

Table 1. Coefficients defining the shape of the micro-aspheric lenslet.

Shape coefficient s	-1
Radius of the array R_0	2.5 mm
Conic constant k	-0.8
Curvature C	0.05 mm^{-1}

Table 2. Machining parameters used for STDM and conventional raster milling.

Machining parameters	STDM	Raster milling
Swing radius (mm)	7.1	7.1
Spindle rotation rate (rpm)	6000	6000
Step distance (μm)	15	15
Tool nose radius (mm)	0.2	0.2
Material	Single-crystal silicon	Single-crystal silicon
Cutting direction	$\langle 100 \rangle$	$\langle 100 \rangle$
Depth of cut (μm)	2	2
Feed rate (mm/min)	22	12,22

5. Results and discussion

To validate the advantages of the proposed STDM system in fabrication of infrared MOAs, micro-aspheric MOAs were machined on a single-crystal silicon wafer using both STDM system and conventional raster milling for comparison. The three-dimensional (3D) surface topography of the 4×3 MOAs generated by STDM is illustrated in Fig. 7(a), and the corresponding microscope diagram of an extracted area is shown in Fig. 7(b). The mirror surface without any brittle fractures or cracks are observed from the whole microscope diagram, which validates the totally ductile cutting mode in STDM of infrared MOAs even under ever-changing cutting depths and local slope. It is also observed that the generated MOAs feature a uniform quality of each lenslet cell in terms of the shape, size and smoothness. The uniform characteristics can be more clearly observed from the 2D cross-sectional profiles traversing the centers of the lenslet along both feed and raster directions, as shown in Figs. 7(c) and 7(d), respectively. A constant spacing distance between two neighboring lenslet cells is also observed along both feed and raster directions. The aperture and the height of each lenslet is at $500 \mu\text{m}$ and $4 \mu\text{m}$, respectively, and the measured values agree well with the desired ones in Table 1.

Since the shape distortion of the lenslet can have a significant impact on the optical performance of MOAs, the enlarged view of an arbitrary lenslet cell was further captured with a $20\times$ amplification, as shown in Fig. 8(a), to evaluate the form accuracy of the generated MOAs. The 2D cross-sectional profiles along x - and y -axis of the machined lenslet are drawn in Figs. 8(b) and 8(c), respectively, to compare with the desired ones defined by Eq. (9). It is observed that the measured profile (blue line) and the desired one (orange line) almost overlap with each other along both directions, and their deviations described by the green lines suggests that the form error is less than $\pm 60 \text{ nm PV}$. To analyze the smoothness and uniformity of the surface quality, the micro-topography of the lenslet cell is obtained through subtracting the aspheric surface from the lenslet cell, as shown in Fig. 8(d), and the microscope image of the lenslet is shown in Fig. 8(e).

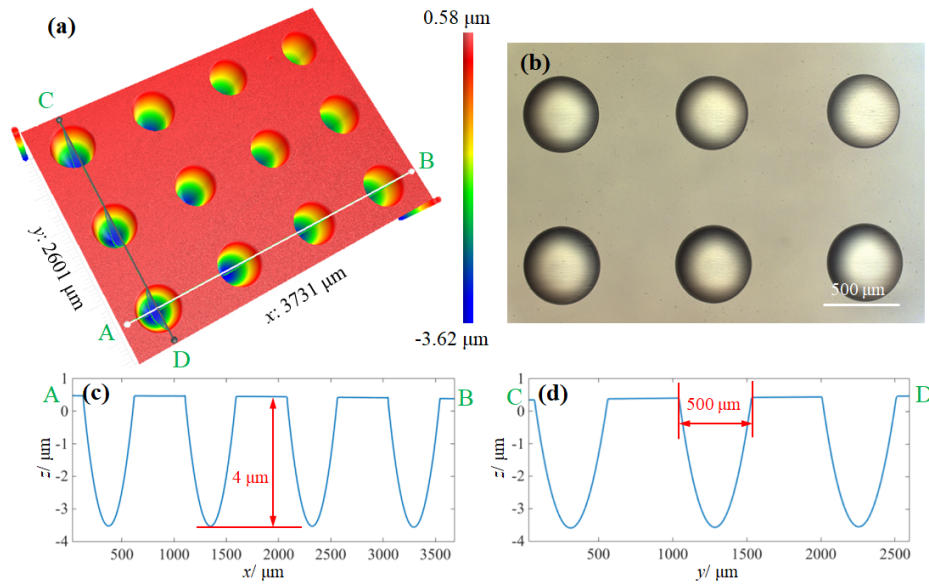


Fig. 7. (a) 3D topography and (b) microscope of the machined MOAs, (c) and (d) the cross-sectional profiles along x - and y -axis, respectively.

The micro-topography is characterized as the homogeneous and crack-free surface quality from its center to the edge field with a very small surface roughness of 4 nm Sa, which demonstrates the effectiveness of the processed to STDM in the fabrication of infrared MOAs with smooth and uniform surface quality. The ribbon-stripe patterns observed in Fig. 8(d) is generated by the intermittent cutting process of STDM [27]. Besides, it also validates that the unique cutting process of STDM well guarantees both the form accuracy and the surface uniformity of the infrared MOAs featuring complicated micro-structured surfaces.

The smooth and uniform surface quality of the generated MOAs is majorly attributed to the unique cutting mechanism of the proposed STDM that applies an extra fast servo motion along feed direction to adaptively match the maximum chip thickness for each tool rotation cycle with the critical DoC. Attributing to this, even though the nominal feed rate in STDM is 22 mm/min equaling to the moving speed of spindle along x -axis, its instantaneous feed rate constantly fluctuates around the nominal one due to the extra self-tuned movement, as discussed in Section 3.2. Consequently, despite of the ever-changing local slope and cutting depths, the maximum chip thickness is strictly equal to the critical DoC of the infrared material in STDM of micro-freeform surfaces, thereby guaranteeing the process consistency and the ductile material removal throughout the whole cutting area. In other words, the STDM is an adaptive cutting process that considers both the form accuracy and the material removal mechanisms. Besides, compared with the famous FTS/STS diamond turning, STDM also process the common advantages of diamond milling when machining infrared materials: (i) the intermittent cutting process of STDM can efficiently suppress the surface damage of infrared material through generating very small chip thickness [25]; (ii) the unchanged feed direction of STDM avoid the adverse radial-spoke marks and inhomogeneous cracks that are easily formed in FTS/STS of single-crystal infrared materials [11,12], as validated in Fig. 7(b) and Fig. 8(e), thereby improving the scattering homogeneity of the infrared optics.

To further validate the unique advantages of the proposed STDM on improving the surface uniformity and machining efficiency in fabrication of infrared MOAs, silicon MOAs were also fabricated by conventional raster milling using different feed rates for comparison, as shown in

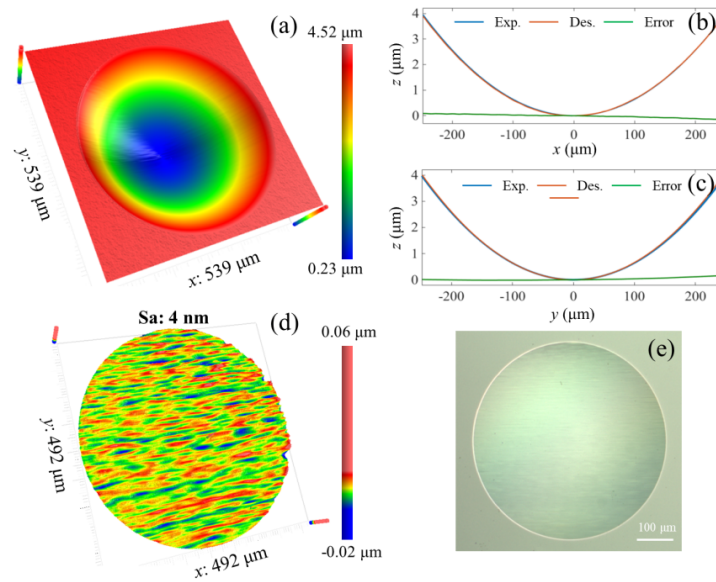


Fig. 8. (a) 3D topography of the lenslet cell, (b) and (c) the corresponding cross-sectional profiles along x and y-axis, (d) micro-topography and (e) microscope.

Fig. 9. Compared with the lenslet obtained by STDM as shown in Fig. 8, obvious brittle fractures can be observed on the downward slope of the lenslet generated by conventional raster milling even using a much smaller feed rate of 12 mm/min, resulting in the non-uniform surface quality and a higher surface roughness of 12 nm, as shown in Figs. 9(b) and 9(c). This is due to the non-adjustable feed rate in conventional milling. In conventional raster milling, the maximum chip thickness for each tool rotational cycle changes from position to position when machining micro-freeform surfaces, as illustrated in Fig. 2. As larger chip thickness can be formed in the downward slope compared with the upward one [11], brittle fractures easily generate in the areas where the cutting depth gradually increases for conventional raster milling. Besides, compared with STDM, a much rougher surface is generated for conventional raster milling even in the ductile cut region, as the microscope images comparatively shown in Fig. 8(e) and Fig. 9(c), which results from the inhomogeneous cutting process of raster milling. In contrast, attributing to the extra servo motion along feed direction in STDM, the instantaneous feed rate in the downward slope region is much slower than that in upward to tune the maximum chip thickness, as illustrated in Fig. 5(d). The adaptive adjustment of the feed rate is the major reason underlying the smoother and more uniform surface quality generated by STDM.

When adopting a larger feed rate at 22 mm/min for conventional milling, more intensive brittle fractures are generated and spread from the downward slope area to the bottom surface of the lenslet, as shown in Figs. 9(d)–9(f). A much higher surface roughness of 43 nm is obtained, as shown in Fig. 9(e). As a result, in order to generate infrared MOAs with crack-free surface, the feed rate for conventional raster milling should be less than 12 mm/min with a spindle rotational speed of 6000 rpm. In contrast, smooth surface without brittle fractures is obtained by STDM even using the nominal feed rate of 22 mm/min, as shown in Fig. 8. Consequently, the nearly double machining efficiency can be achieved by STDM compared with the conventional one.

It is known that rough cutting is normally adopted when machining optical freeform surfaces with the azimuthal height variation over hundreds or even thousands of micrometers, to avoid the severe tool vibrations at large depth-of-cut. As the allowable cutting depth for ultra-precision diamond cutting is generally ranges from sub-micrometer to tens of micrometers, one-step

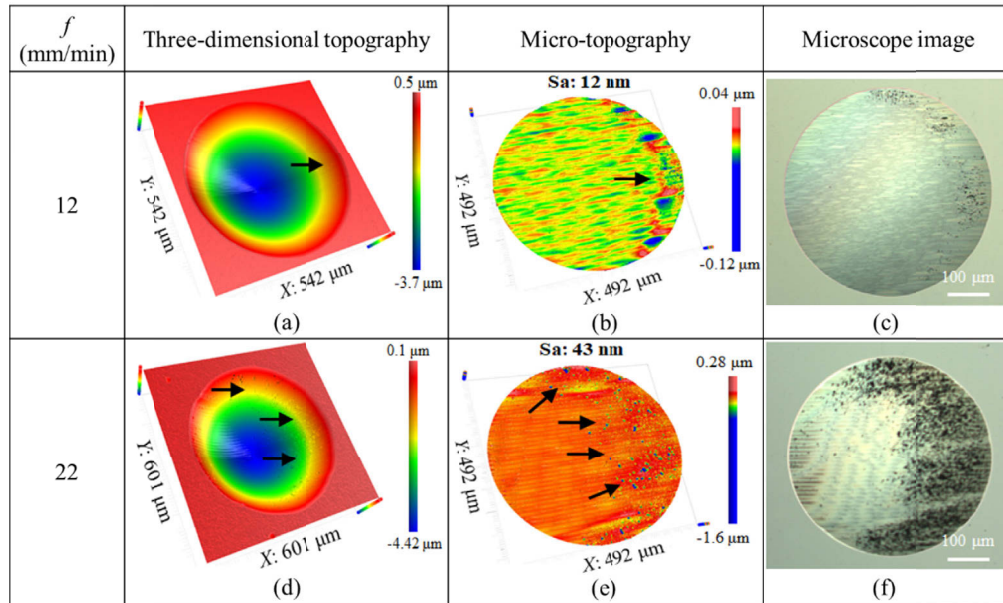


Fig. 9. 3D surface topographies, micro-topographies and microscopes of the lenslet generated by raster milling under different feed rates.

operation is normally adopted when diamond cutting micro-structured surfaces with small azimuthal height variation as the MLAs fabricated in this manuscript to improve the machining efficiency. Besides, unlike machining the optical mold on copper or aluminum in which case rough cutting can be adopted, repeat cutting operation will lead to the propagation of micro-cracks of infrared materials and finally deteriorate the finished surface quality, so one-step cutting operation is more beneficial to guarantee the optical performance for infrared optics [25]. The proposed STDM can achieve the one-step generation of infrared MOAs with uniform and crack-free surface quality through self-adaptively matching the maximum chip thickness for each tool rotational cycle with the critical depth of cut of the infrared material according to the local surface topography.

The employment of total integrated scattering (*TIS*) as the index to evaluate the optical performance of infrared optics is widely accepted by researchers as in Ref. [11,16,28], and *TIS* can be calculated by:

$$TIS \approx \left(\frac{4\pi\delta}{\lambda}\right)^2 \quad (10)$$

where δ is the root-mean-square value of the surface deviation that can be roughly equal to 1.25 times surface roughness, λ denotes the wavelength of the incident light ranging from 6 to 1.2 μm for single-crystal silicon. As declared by Harvey *et al.* [28], *TIS* should be less than 0.01 to guarantee the optical performance for most optical components, thus the surface roughness no larger than 9 nm is mandatory for the infrared MOAs made by silicon. Consequently, the surface roughness of 4 nm achieved by the proposed STDM fulfils the highest requirement of the infrared MOAs made by silicon covering the entire infrared region, while the surface roughness of 12 nm obtained by conventional milling is unsatisfactory even using a much smaller feed rate. Apart from surface roughness, the form accuracy of an optical component normally needs to be less than a quarter of λ [29], thus the form accuracy the silicon MOAs is required to be less than 300 nm. The form accuracy of the lenslet machined by STDM is ± 60 nm in the present study also satisfy the requirements.

Essentially, the geometrical feature of any micro-optics arrays is the ever-changing height and slop of the micro-structured surfaces, including all of the concave micro-lens, convex micro-lens and micro pyramids arrays. As demonstrated in the manuscript, the major advantage of the proposed STDM is its self-tuned nature that can self-adaptively match the maximum chip thickness for each tool rotational cycle with the critical depth of cut of the infrared material according to the local height and slop of the machined micro-optics arrays. Thus, STDM is applicable to any micro-optics arrays featuring ever-changing height and slop.

6. Conclusions

To achieve the ductile cutting of infrared micro-optics arrays (MOA) with high surface uniformity and enhanced machining efficiency, a novel self-tuned diamond milling (STDM) system is proposed in this study through integrating a dual-axial fast servo motion platform into a diamond raster milling system. With the assistance of the dual-axial fast servo motions along both feed and depth-of-cut (DoC) directions, the maximum chip thickness for each tool rotational cycle in STDM is self-adaptively tuned to be strictly equal to the critical DoC of the infrared material while generating micro-freeform lenslet, thereby guaranteeing both the smoothness and uniformity of the whole MOAs as well as improving machining efficiency. The corresponding toolpath planning algorithm is also proposed with the full consideration of the tool geometry, the unique kinematics of the STDM system and the infrared material property. The proposed STDM efficiently overcomes the inherent limitations for the existing diamond cutting technologies on the avoidance of the local fractures and the improvement of the feed rate when machining micro-structured optics on infrared materials. The key conclusions are as follows:

- (1) The employment of the dual-axial fast servo motions provides the STDM system with high flexibility in terms of the toolpath planning algorithm that can consider both the form accuracy of the desired MOAs and the material removal mode of the infrared material. The density of the determined swing center points (SCP) changes with respect to the instantaneous cutting depth and local slope.
- (2) In STDM, the relative motion between the SCP and the workpiece can be decomposed into the uniform motion of the spindle and the oscillations of the self-tuned fast servo motions. The resulting fluctuations of the instantaneous feed rate is responsible for the self-adaptively matching the maximum chip thickness with the critical DoC.
- (3) To validate the proposed STDM, a crack-free micro-aspheric MOAs is successfully machined on single-crystal silicon with the form error of ± 60 nm. Compared with the conventional milling, a smoother and more uniform surface quality with the smaller surface roughness of 4 nm is achieved by STDM for each lenslet, attributing to the processing consistency of STDM.
- (4) Extremely small feed rates are normally required for conventional milling to avoid fractures generated at the downward slope and large DoC regions. In comparison, the self-tuned feature of STDM can highly increase the average feed rate while ensuring the smoothness, and nearly double machining efficiency is improved by STDM.

Funding

National Natural Science Foundation of China (51675455, 51975128); Shenzhen Science and Technology Innovation Commission (JCYJ20160427184134564).

Acknowledgments

This work was supported partially by the State Key Laboratory of Ultra-precision Machining Technology. We thank Prof. To for the guidance and support on the experiments.

Disclosures

The authors declare no conflicts of interest.

References

1. Z. Hong and R. Liang, "IR-laser assisted additive freeform optics manufacturing," *Sci. Rep.* **7**(1), 7145 (2017).
2. C. Deng, H. Kim, and H. Ki, "Fabrication of a compound infrared microlens array with ultrashort focal length using femtosecond laser-assisted wet etching and dual-beam pulsed laser deposition," *Opt. Express* **27**(20), 28679–28691 (2019).
3. W.-L. Zhu, F. Duan, X. Zhang, Z. Zhu, and B.-F. Ju, "A new diamond machining approach for extendable fabrication of micro-freeform lens array," *Int. J. Mach. Tool. Manu.* **124**, 134–148 (2018).
4. G. Yan, Y. Zhang, K. You, Z. Li, Y. Yuan, and F. Fang, "Off-spindle-axis spiral grinding of aspheric microlens array mold inserts," *Opt. Express* **27**(8), 10873–10889 (2019).
5. Z. Zhu, X. Zhou, D. Luo, and Q. Liu, "Development of pseudo-random diamond turning method for fabricating freeform optics with scattering homogenization," *Opt. Express* **21**(23), 28469–28482 (2013).
6. A. Krywonos, J. E. Harvey, and N. Choi, "Linear systems formulation of scattering theory for rough surfaces with arbitrary incident and scattering angles," *J. Opt. Soc. Am. A* **28**(6), 1121–1138 (2011).
7. H. Zuo, D.-Y. Choi, X. Gai, B. Luther-Davies, and B. Zhang, "CMOS compatible fabrication of micro, nano convex silicon lens arrays by conformal chemical vapor deposition," *Opt. Express* **25**(4), 3069–3076 (2017).
8. Y. Zhang, J. Luo, Z. Xiong, H. Liu, L. Wang, Y. Gu, Z. Lu, J. Li, and J. Huang, "User-defined microstructures array fabricated by DMD based multistep lithography with dose modulation," *Opt. Express* **27**(22), 31956–31966 (2019).
9. Z. Li, F. Fang, J. Chen, and X. Zhang, "Machining approach of freeform optics on infrared materials via ultra-precision turning," *Opt. Express* **25**(3), 2051–2062 (2017).
10. D. Li, B. Wang, Z. Qiao, and X. Jiang, "Ultraprecision machining of microlens arrays with integrated on-machine surface metrology," *Opt. Express* **27**(1), 212–224 (2019).
11. M. Mukaida and J. Yan, "Ductile machining of single-crystal silicon for microlens arrays by ultraprecision diamond turning using a slow tool servo," *Int. J. Mach. Tool. Manu.* **115**, 2–14 (2017).
12. M. Wang, W. Wang, and Z. Lu, "Anisotropy of machined surfaces involved in the ultra-precision turning of single-crystal silicon—a simulation and experimental study," *Int. J. Adv. Manuf. Technol.* **60**(5-8), 473–485 (2012).
13. Z. Sun, S. To, G. Zhang, and S. Zhang, "Flexible fabrication of micro-optics arrays with high-aspect-ratio by an offset-tool-servo diamond machining system," *Opt. Express* **27**(7), 9631–9646 (2019).
14. Z. Zhu and S. To, "Adaptive tool servo diamond turning for enhancing machining efficiency and surface quality of freeform optics," *Opt. Express* **23**(16), 20234–20248 (2015).
15. Z. Zhu, S. To, and S. Zhang, "Large-scale fabrication of micro-lens array by novel end-fly-cutting-servo diamond machining," *Opt. Express* **23**(16), 20593 (2015).
16. Z. Sun, S. To, and K. Yu, "One-step generation of hybrid micro-optics with high-frequency diffractive structures on infrared materials by ultra-precision side milling," *Opt. Express* **26**(21), 28161–28177 (2018).
17. B. S. Dutterer, J. L. Lineberger, P. J. Smilie, D. S. Hildebrand, T. A. Harriman, M. A. Davies, T. J. Suleski, and D. A. Lucca, "Diamond milling of an Alvarez lens in germanium," *Precis. Eng.* **38**(2), 398–408 (2014).
18. J. Owen, J. Troutman, T. Harriman, A. Zare, Y. Wang, D. Lucca, and M. Davies, "The mechanics of milling of germanium for IR applications," *CIRP Ann.* **65**(1), 109–112 (2016).
19. Z. Sun, S. To, and S. Zhang, "A novel ductile machining model of single-crystal silicon for freeform surfaces with large azimuthal height variation by ultra-precision fly cutting," *Int. J. Mach. Tool. Manu.* **135**, 1–11 (2018).
20. Z. Sun, S. To, and K. Yu, "An investigation in the ultra-precision fly cutting of freeform surfaces on brittle materials with high machining efficiency and low tool wear," *Int. J. Adv. Manuf. Technol.* **101**(5-8), 1583–1593 (2019).
21. A. Mir, X. Luo, K. Cheng, and A. Cox, "Investigation of influence of tool rake angle in single point diamond turning of silicon," *Int. J. Adv. Manuf. Technol.* **94**(5-8), 2343–2355 (2018).
22. Z. Zhu, S. To, G. Xiao, K. F. Ehmman, and G. Zhang, "Rotary spatial vibration-assisted diamond cutting of brittle materials," *Precis. Eng.* **44**, 211–219 (2016).
23. S. Wang, J. Wang, X. Lei, Z. Liu, J. Zhang, and Q. Xu, "Investigation of the laser-induced surface damage of KDP crystal by explosion simulation," *Opt. Express* **27**(11), 15142–15158 (2019).
24. G. Xiao, S. To, and E. Jelenković, "Effects of non-amorphizing hydrogen ion implantation on anisotropy in micro cutting of silicon," *J. Mater. Process. Technol.* **225**, 439–450 (2015).
25. Z. Sun, S. To, and K. Yu, "Feasibility investigation on ductile machining of single-crystal silicon for deep micro-structures by ultra-precision fly cutting," *J. Manuf. Process.* **45**, 176–187 (2019).
26. D. Yu, Y. Wong, and G. Hong, "Ultraprecision machining of micro-structured functional surfaces on brittle materials," *J. Micromech. Microeng.* **21**(9), 095011 (2011).

27. S. J. Zhang, S. To, and S. J. Zhang, "The effects of spindle vibration on surface generation in ultra-precision raster milling," *Int. J. Mach. Tool. Manu.* **71**, 52–56 (2013).
28. J. E. Harvey, S. Schröder, N. Choi, and A. Duparré, "Total integrated scatter from surfaces with arbitrary roughness, correlation widths, and incident angles," *Opt. Eng.* **51**(1), 013402 (2012).
29. H. Ottevaere, R. Cox, H.-P. Herzig, T. Miyashita, K. Naessens, M. Taghizadeh, R. Völkel, H. Woo, and H. Thienpont, "Comparing glass and plastic refractive microlenses fabricated with different technologies," *J. Opt. A: Pure Appl. Opt.* **8**(7), S407–S429 (2006).